RESEARCH ARTICLE

Experimental investigation of yaw-angle effects on drag reduction rate for trapezoidal riblets

Ayumu Inasawa[1] · Ryo Taniguchi[1] · Masahito Asai[1] · Monami Sasamori[2] · Mitsuru Kurita[2]

Abstract

Effects of the yaw angle on the drag reduction rate of riblets were investigated experimentally for trapezoidal riblets with ridge angle of 30° and height-to-spacing ratio of 0.5 in a turbulent wind channel at Reynolds numbers (based on the friction velocity and channel half depth) $Re_\tau = 520 - 2100$. Drag reduction rates were estimated carefully by comparing the streamwise pressure gradients between turbulent channel flows with and without riblets. The maximum drag reduction rate which was about 7% for the streamwise riblets was maintained without any attenuation for the yaw angle ϕ below 10°. When ϕ exceeded 10°, the drag reduction rate was attenuated steeply and the performance of riblets was almost lost at $\phi = 15°$. The yaw angle at which the drag turned to increase was by 10° smaller than the value reported for the saw-tooth riblets. The yaw angle effect on the riblet performance was further examined by detailed comparisons of mean velocity profiles and turbulent structures near the ribbed surfaces for $\phi = 10°$ and 15°. Although no appreciable difference in the turbulent intensity and pre-multiplied spectrum of near-wall turbulence was found between these cases ($\phi = 10°$ and 15°), the mean velocity profile for the case of $\phi = 15°$ indicated an evidence of flow separation at the ridges of riblets, leading to the attenuation of drag-reduction rate due to increase in the pressure drag.

1 Introduction

Surface manipulation with riblets (or longitudinal grooves) is one of the most successful passive means to reduce friction drag in wall turbulence. Since early work by Walsh and Weinstein (1978) and Walsh (1980a, 1983), several cross-sectional geometries of riblets (or grooves) such as sawtooth, scalloped, blade and trapezoidal ones have been

✉ Ayumu Inasawa
    ainasawa@tmu.ac.jp

    Ryo Taniguchi
    rtaniguchi@aero.sd.tmu.ac.jp

    Masahito Asai
    masai@tmu.ac.jp

    Monami Sasamori
    sasamori.monami@jaxa.jp

    Mitsuru Kurita
    kurita.mitsuru@jaxa.jp

[1] Department of Aeronautics and Astronautics, Tokyo Metropolitan University, 6-6 Asahigaoka, Hino, Tokyo 191-0065, Japan

[2] Aviation Technology Directorate, Japan Aerospace Exploration Agency, Osawa, Mitaka, Tokyo 181-0015, Japan

proposed and their drag reduction effects and underlying mechanism have been examined experimentally and numerically (Bechert and Bartenwerfer 1989; Choi 1989; Walsh 1980b; Choi et al. 1993; Suzuki and Kasagi 1994; Wang et al. 2000). For all the groove geometries of riblets, the drag reducing effect is divided into three regimes. In the viscous regime of $s^+ \leq 10$–15 (where s^+ is riblet spacing in wall units), turbulent vortices have no significant impact on the flow inside grooves, and thus the viscous sublayer over the riblets is laminar-like. In this regime, the drag reduction rate due to a viscous effect is linearly proportional to s^+ (Bechert and Bartenwerfer 1989; Luchini et al. 1991). Beyond this value of s^+, the so-called viscous breakdown occurs and the drag reducing effect of riblets is saturated at $s^+ = 15$–20 due to increase in the turbulent Reynolds stress near the riblets (Garcia-Mayoral and Jiménez 2011a). When s^+ is further increased, the drag reducing effect of riblets is weakened with s^+ (although riblets still affect activity of near-wall turbulence) and finally the friction drag turns to increase (compared to the smooth surface case), that is, riblets act as roughness. The maximum drag reduction rate realized by riblets is thus controlled by the viscous effect and viscous breakdown phenomenon, both of which depend on the riblet geometry. The maximum drag reduction rate was found to be

5% (for triangular/sawtooth riblets) to 10% (for blade riblets) for the height to spacing ratio $s/h = 0.5$ and the optimal size of the riblet cross section was over 10–20 in wall units in terms of the distance between neighboring ridges, depending on the riblet geometry, as summarized by Bechert et al. (1997) and Garcia-Mayoral and Jiménez (2011b). Here, concerning the optimal riblet size, Garcia-Mayoral and Jiménez (2011a) found that when the riblet-ridge spacing was represented by the square root of the groove cross-sectional area in wall units $(A_g^+)^{1/2}$, the maximum drag reduction occurred at $(A_g^+)^{1/2} \approx 10.7 \pm 1$ for all groove geometries. This scaling was also confirmed by von Deyn et al. (2022).

For practical application of riblets to aircraft, on the other hand, it is also important to understand impacts of yaw angle of riblets ϕ (angle between mean flow and riblets) on the drag reducing effects or the sensitivity of the drag reduction to flow misalignment because the drag-reducing effect can be attenuated by additional pressure drag due to flow separating at riblet-ridges in case of flow misalignment. In this concern, Sundaram et al. (1999) applied streamwise riblets to a 25°-swept-wing in a subsonic wind tunnel experiment and reported that flow misalignment due to large cross flow velocity could degrade the riblet performance. Walsh (1982) first examined the yaw effect experimentally for the sawtooth (triangular) riblets (with $s/h = 0.5$) and found that the drag reduction rate was nonsensitive to the flow misalignment even at $\phi = 15°$ and the drag reduction performance of riblets was expected up to $\phi = 25$; also see Walsh and Lindemann (1984). This value $\phi = 15°$ has often been cited as the critical yaw angle of riblets for nonsensitivity to the misalignment. Understanding of yaw-angle effect of riblets is also important for designing non-straight riblets such as spanwise wavy riblets for which some increase in the maximum drag reduction by 1–2% compared to the straight riblets was reported (Peet and Sagaut 2009; Sasamori et al. 2014; Okabahashi et al. 2015; Sasamori et al. 2017; Cafiero and Ius 2022). Concerning other riblet geometries, Hage et al. (2001) examined the yaw angle effect for triangular, semicircular and trapezoidal grooves by measuring the drag of yawed riblets glued on a circular plate directly using a shear stress balance in an oil channel. Their results showed that the drag reduction rate was gradually attenuated with increasing the yaw angle for all groove geometries, without a distinct threshold below which the drag reduction rate was not attenuated, which was different from the Walsh's result. Okabayashi (2017) conducted a direct numerical simulation for trapezoidal riblets with ridge angle of 30° at a low turbulent Reynolds number $Re_\tau = 180$ and reported that the advantage of drag reduction was kept until ϕ exceeded 20°, although the simulations were conducted only for $s^+ \geq 17$.

In the present study, effects of the yaw angle on the drag reduction rate of riblets are carefully examined for trapezoidal riblets with 30°-ridges experimentally in turbulent wind channel to see how critically the drag reducing effect of riblets is attenuated by the flow misalignment. In channel flows over ribbed surface, comparison of drag with the smooth surface may depend on the (virtual) wall location, especially for yawed riblets. In order to reduce uncertainty in the determination of the virtual wall position, the present experiment was conducted at the Reynolds number (based on the friction velocity and channel half depth) of 520–2100 in the channel whose depth was 240 times larger than riblet height.

2 Experimental setup

The whole experiment was conducted in a turbulent wind channel whose length (L), depth ($2H$) and spanwise width (W) were 10 m, 100 mm, and 900 mm, respectively, giving the aspect ratio of the channel cross section of 9. The flow was driven by a counter-rotating axial fan. The center-line velocity U_c can be changed up to about 45 m/s continuously: The maximum Reynolds number defined as $Re_c = U_c H/\nu$ (where ν is the kinematic viscosity) was 1.50×10^5. As for the coordinate system, x was the streamwise distance measured from the channel inlet, y the normal-to-wall distance and z the spanwise distance; see Fig. 1a. Both channel walls ($L \times W$ area) were made of transparent and highly-flat-5-mm-thick glass-plates in order to keep the channel cross section to be constant in the streamwise direction, in addition to the optical access from outside the channel walls. The end walls ($L \times 2H$ area) were of 20-mm-thick Aluminum plate. Note that the channel was set vertically. The channel glass walls were supported rigidly by Aluminum frames attached to the glass walls at an equal interval of 250 mm to avoid deformation of the glass walls due to higher static pressure inside the channel than the outside atmospheric pressure; see Fig. 1b. The channel had 40 pressure taps (0.4 mm in diameter and 3 mm in depth) with an equal interval of 250 mm in the streamwise direction over 125 mm $\leq x \leq$ 9875 mm. The pressure taps were drilled 225 mm apart from the spanwise mid position ($z = 225$ mm). To promote transition to fully-developed wall turbulence, the inlet flow was tripped at the channel entrance ($x = 200$ mm) by gluing two rows of cylinder-roughness elements (height of 5 mm, diameter of 4 mm) in a staggered manner on the both walls in the whole span.

Riblets had triangular ridges with a ridge angle of 30° and trapezoidal valleys, as illustrated in Fig. 2a. The riblets were manufactured by means of resin mold. The ridge spacing s and height h were 0.83 and 0.415 mm (= 0.5s), respectively, giving the ratio of the groove cross-sectional area A_g to the square of the spacing $A_g/s^2 = 0.43$. Note that

Fig. 1 Turbulent wind channel apparatus. **a** Schematic diagram. **b** Sideview and **c** end-view photographs of wind channel with ribbed wall installation in the test section
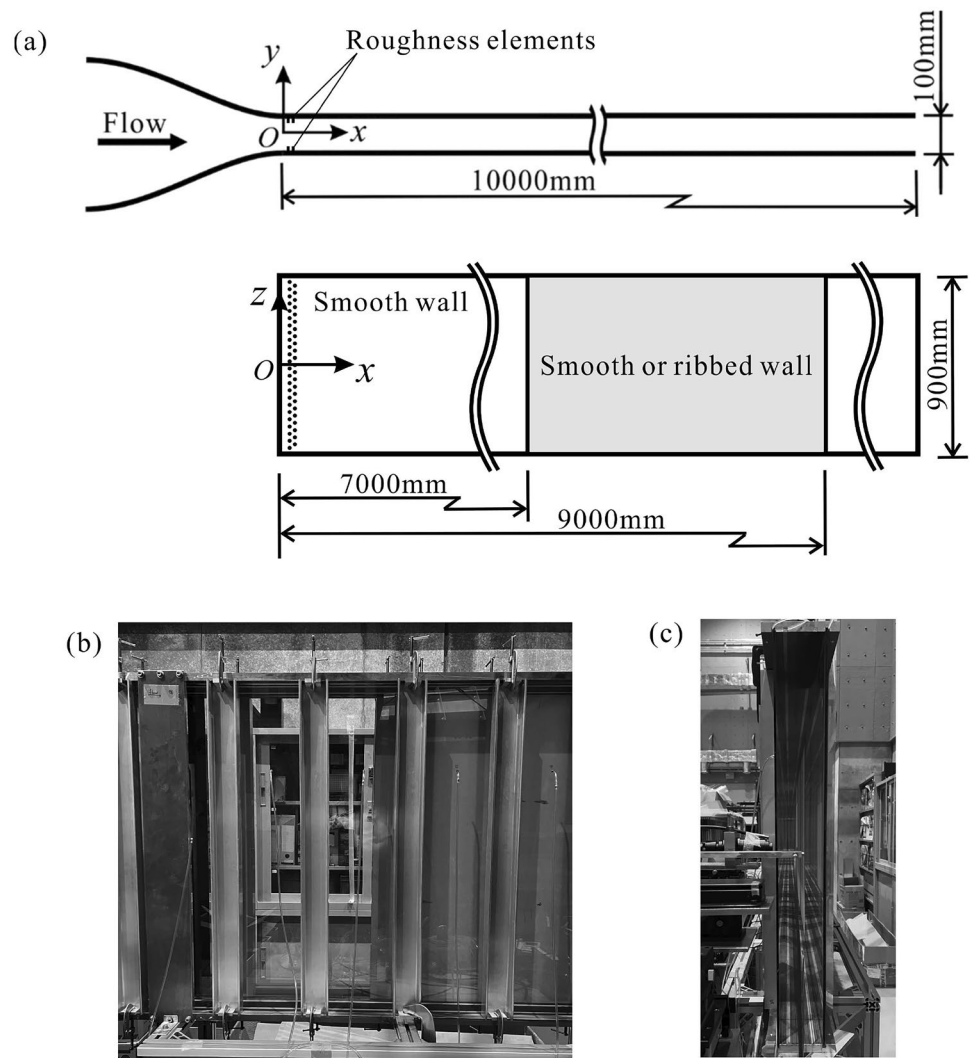
the tip thickness of riblet ridges was 0.005 mm. Photographs of the trapezoidal riblets used are displayed in Fig. 2b. Four different riblet-ridge alignments were employed; one was parallel to the mean flow, i.e., streamwise riblets ($\phi = 0°$) and the other three were yawed to the mean flow direction, with the yawed angle $\phi = 10°$, 12.5° and 15° as shown in Fig. 3. A riblet plate (riblet sheets of 2 m long and 400 mm wide were glued on a 2-m-long glass plate) was connected to the upstream smooth-surface plate in such a way that the bottom of riblet-grooves was placed at the same position as the upstream smooth surface. The virtual origin at which the mean velocity profile approached zero would be about 0.4h (~ 0.2 mm) below the tip of the ridges for streamwise riblets having 30°-ridge and trapezoidal grooves (Luchini et al. 1991). In such a case, the change in the channel cross-sectional area would be only 0.3% of the channel depth ($2H = 100$ mm) and thus the influence of the change in the cross-sectional area would be negligibly small on the

comparison of friction drag between the smooth and ribbed surface channels in the present experiment.

Drag reduction rate was estimated by comparing pressure losses (more exactly speaking, the pressure gradient in the streamwise direction) between the smooth and ribbed surfaces in the downstream test section beyond $x = 7000$ mm. The static pressure was measured using high-precision pressure transducer (Validyne). The output signal was stored in a PC via Analog-to Digital (A/D) converter (NI) with sampling frequency and sampling duration being 1000 Hz and 50 s, respectively. In order to minimize possible influences of difference in kinetic viscosity in a pair of measurements for smooth and ribbed surfaces, temperature and atmospheric pressure in the laboratory were monitored. The centerline velocity U_c which defined the Reynolds number Re was measured at the channel exit. In this concern, it should be noted that in the experiment on drag reduction rates of riblets, there is 1-m-long smooth surface region (from $x = 9$–10 m) downstream of the riblets wall ($x = 7$–9 m) and thus

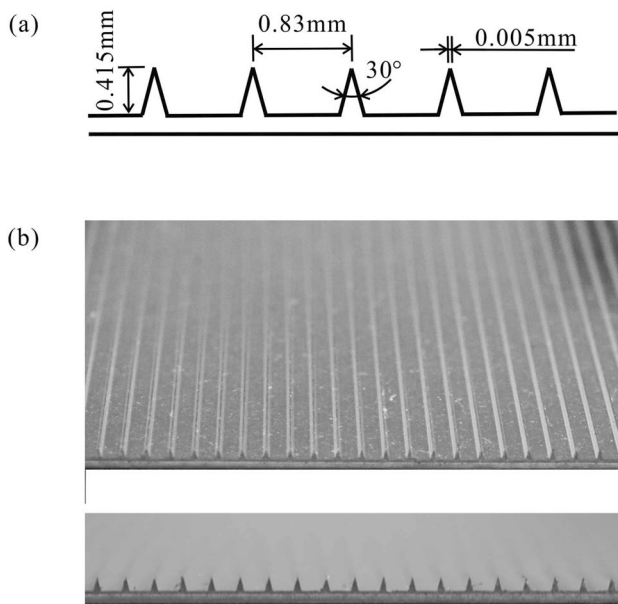Fig. 2 **a** Schematic diagram of riblet cross section. **b** Photographs of streamwise riblets

Fig. 4 Photograph of hot-wire rake probe with 48 sensors

the flow no doubt returned to that on smooth surface near the channel exit. Thus, in the comparison of the pressure gradient in the smooth and ribbed channels, when the center velocity U_c coincides with each other (with and without riblets cases), we may expect that the flow rates were the same in both cases. The center velocity was set carefully to reproduce the same flow condition for both cases; the drag reduction rate of riblets was examined in the flow condition in which the difference in the centerline velocity in both cases was less than 0.05% of U_c.

The streamwise velocity component $(U + u)$ where U and u denote the time-mean and fluctuation components, respectively, was measured using a low-noise constant temperature hot-wire anemometer (Inasawa et al. 2020, 2021). A hot-wire probe was inserted into the flow from the downstream end of the channel. The sensitive length of hot wire sensor (5-μm-tungsten wire) was 1 mm. A digital microscope (HOZAN) whose working distance from the object

to the lens front was 105 mm was employed to monitor/detect the sensor position relative to the tip of riblet ridges. The microscope was installed on a high-precision traversing mechanism with spatial resolution of 0.5 μm (SIGMA). The sensor position could be determined with accuracy of ± 10 μm, about $\pm 2.5\%$ of the riblet height h or ± 0.2 in wall units for $s^+ \approx 15$, in such a way that the sensor and riblet-edges were, respectively, in focus. In addition, a hot-wire rake probe with high spatial resolution was used to visualize and analyze turbulent structures in the $x - z$ plane near the ribbed surfaces where a conventional PIV was not available. The rake probe had 48 hot-wire sensors aligned in the spanwise direction at an equal interval of 0.6 mm, as displayed in Fig. 4. This hot-wire rake was operated with a constant current mode.

In order to change the riblet-ridge spacing in wall units $s^+ = s u_\tau / \nu$, the mean streamwise velocity at the channel center U_c was changed from 3 to 13 m/s. Then, the riblet-ridge spacing in wall units $s^+ = s u_\tau / \nu$ varied from 7 to 33, where u_τ was the friction velocity on the smooth surface. Correspondingly, the turbulent Reynolds number $\mathrm{Re}_\tau = H u_\tau / \nu$ ranged over 520–2100.

Fig. 3 Photographs of yawed riblets (plan view). **a** $\phi = 10°$, **b** $\phi = 15°$. The cross-sectional geometry is the same as that in Fig. 2

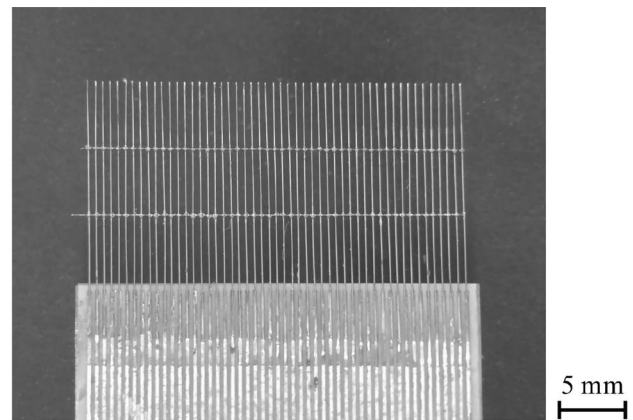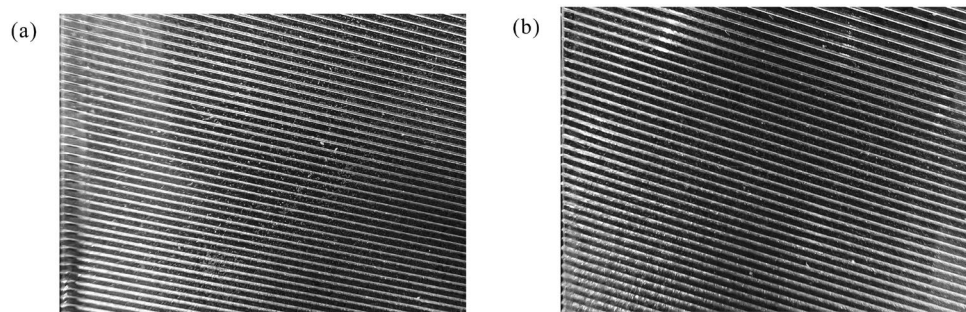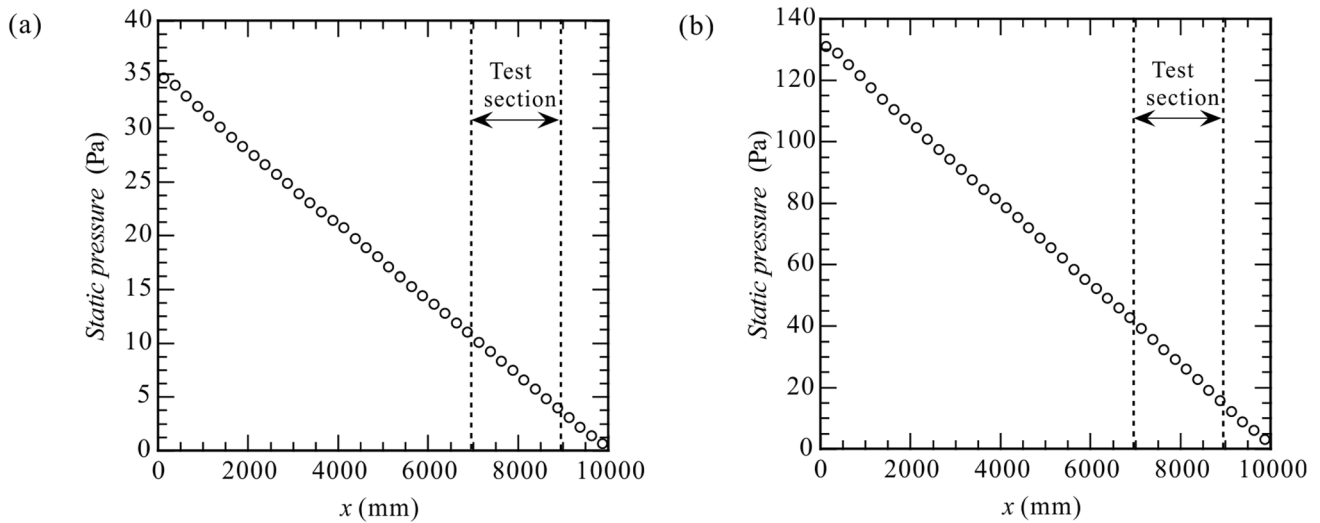**Fig. 5** Streamwise variation of static pressure p in the smooth-surface channel at **a** $U_c = 9.87$ and **b** 12.5 m/s (Re$_c = 3.22 \times 10^4$ and 4.06×10^4)

3 Results and discussion

In this section, experimental results are presented and discussed. Results include comparisons of streamwise distribution of static pressure between smooth and ribbed surfaces, comparisons of drag reduction rates between streamwise and yawed riblets and normal-to-surface distributions of mean velocity and rms value of turbulence near the streamwise and yawed riblets.

3.1 Mean flow and streamwise distribution of static pressure

Figure 5 displays streamwise variations of (time-mean) static pressure of flows in the smooth-surface channel

at the channel center velocity $U_c = 9.87$ and 12.5 m/s which gave the Reynolds numbers Re$_c = 3.22 \times 10^4$ and 4.06×10^4, respectively. We see that the pressure gradient has approached a constant value beyond a location about 2000 mm ($= 40H$) downstream of the inlet for each case. To confirm that the flow is fully developed in the downstream text section, mean flow profiles and rms distributions of turbulent fluctuations on the smooth surface were measured at $x = 9900$ mm. In Fig. 6a, b, the y-distributions of mean velocity U and rms value of streamwise velocity fluctuation u' at the turbulent Reynolds number Re$_\tau = 520$ are compared to the corresponding DNS results (Moser et al. 1999) made at a close Reynolds number. Here, the friction velocity was obtained from the velocity profile. Both U- and u'-profiles agree well with the DNS results,
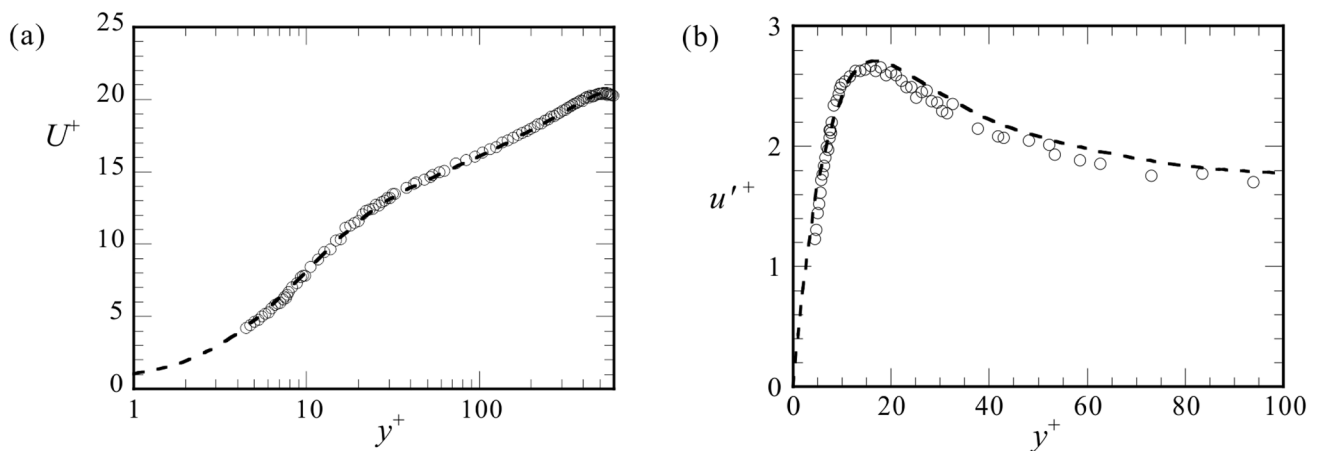

Fig. 6 The y-distributions of **a** mean velocity U and **b** rms value of streamwise velocity fluctuation u' in the smooth-surface channel (Re$_\tau = 520$). Dashed lines represent DNS (Moser et al. 1999) (Re$_\tau = 590$)

confirming that the turbulent flow tripped by roughness elements was fully developed in the downstream test section. Note that a difference in the y^+-distributions of u'^+ was due to the slight difference in Re_τ.

3.2 Drag reduction rate of streamwise riblets

Streamwise variations of (time-mean) static pressure of the turbulent channel flows with and without streamwise riblets measured at $\mathrm{Re}_\tau = 1090$ and 1870 are compared in Fig. 7a, b, respectively; here, the riblet spacing s^+ was 18 and 32 in these conditions, respectively. When the flow entered the riblet region ($x \geq 7000$ mm), we can see a slight difference in the streamwise variation of static pressure between the smooth and ribbed surfaces for $\mathrm{Re}_\tau = 1090$ ($s^+ = 18$ for riblets). The pressure gradient in the riblet case was smaller than that for the smooth-surface case, showing that the turbulent drag was reduced by the riblets. For $\mathrm{Re}_\tau = 1870$ ($s^+ = 32$ for riblets), on the other hand, the pressure gradient was nearly the same between the smooth and ribbed surfaces in the whole distance, indicating that the drag reducing effect disappeared for $s^+ = 32$. Here, it should be noted that the influence of sudden change in the surface condition (from smooth to ribbed) at $x = 7000$ mm lasted about 1000 mm downstream, that is, it took a distance of $20H$ for the pressure gradient to become constant. In this concern, we may refer to an experiment on the downstream influences of a step-like change in rough surface in a turbulent pipe flow (Van Buren et al. 2020), in which the pressure gradient attains the equilibrium state about 20 radii downstream of the step change. The distance is the same as that in the present experiment

($\sim 20H$). Therefore, in the present experiments, streamwise variations of static pressure over 7875 mm $\leq x \leq 8875$ mm (distance of five pressure taps) were adopted to evaluate the turbulent drag of the ribbed surface τ_{riblet}, while the pressure distributions over 7375 mm $\leq x \leq 8875$ mm (seven pressure taps) were used to obtain the turbulent drag for the smooth surface τ_{smooth}. Note that the pressure gradient dp/dx was obtained by the 1st-order least-square method for the measured pressure data.

The drag reduction rate $\Delta\tau$ was defined as,

$$\Delta\tau = \frac{\tau_{\mathrm{riblet}} - \tau_{\mathrm{smooth}}}{\tau_0}, \tag{1}$$

where τ_{smooth} and τ_{riblet} represent the wall shear stresses on the smooth and ribbed surface, respectively, and τ_0 is the wall shear stress at the mid-span of the smooth channel. τ_{smooth} was obtained from the pressure gradient (or the pressure drop per 1 m) as,

$$\tau_{\mathrm{smooth}} = -\frac{WH}{W + 2H}\left(\frac{dp}{dx}\right)_{\mathrm{smooth}} = -\frac{9H}{10}\left(\frac{dp}{dx}\right)_{\mathrm{smooth}} \tag{2}$$

because $W = 18H$. Here, it should be noted that the pressure drop is balanced with the friction drag of four channel walls (left, right and two side walls) so that the wall shear stress τ_{smooth} might include a non-negligible influence from the side walls because the aspect ratio of the present channel ($= 9$) is not sufficiently large. In order to understand the effect from the side walls on the friction drag, we examined local friction (wall shear stress) over the cross section of the channel by means of the Preston tube method (Preston 1954; Patel 1965). Figure 8a, b illustrates the y- and
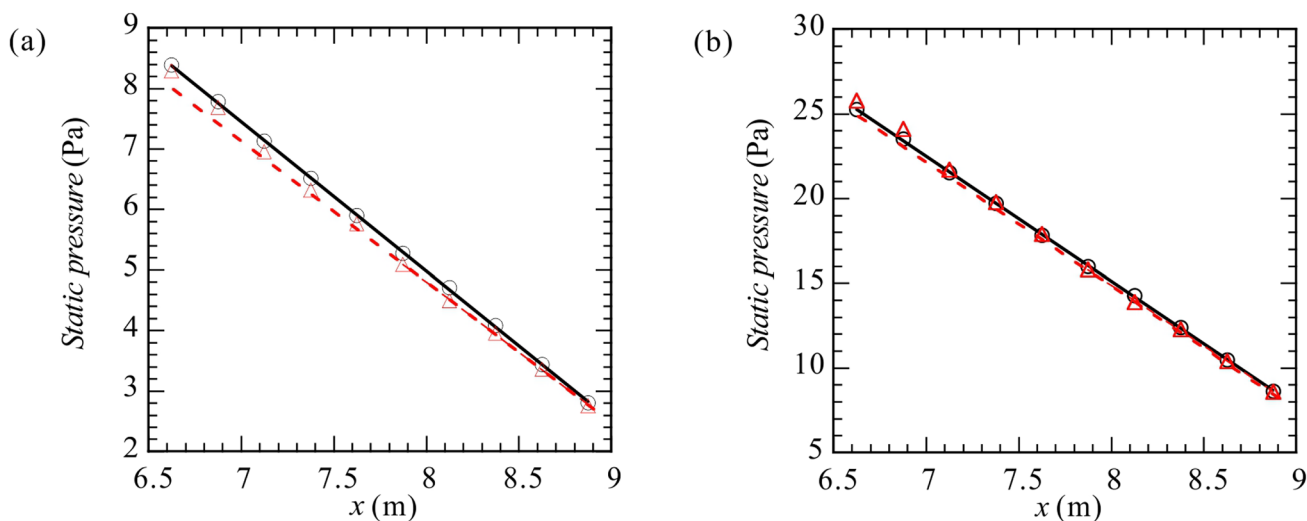

(a)

(b)

Fig. 7 Comparisons of streamwise variations of static pressure with and without streamwise riblets ($\phi = 0$). Symbols of circle (black) and triangle (red) represent smooth and streamwise riblets, respec-tively. Slope of lines represents the values of dp/dx. **a** $\mathrm{Re}_\tau = 1090$ ($U_c = 7.01$ m/s, $s^+ = 18$). **b** $\mathrm{Re}_\tau = 1870$ ($U_c = 13.1$ m/s, $s^+ = 32$)
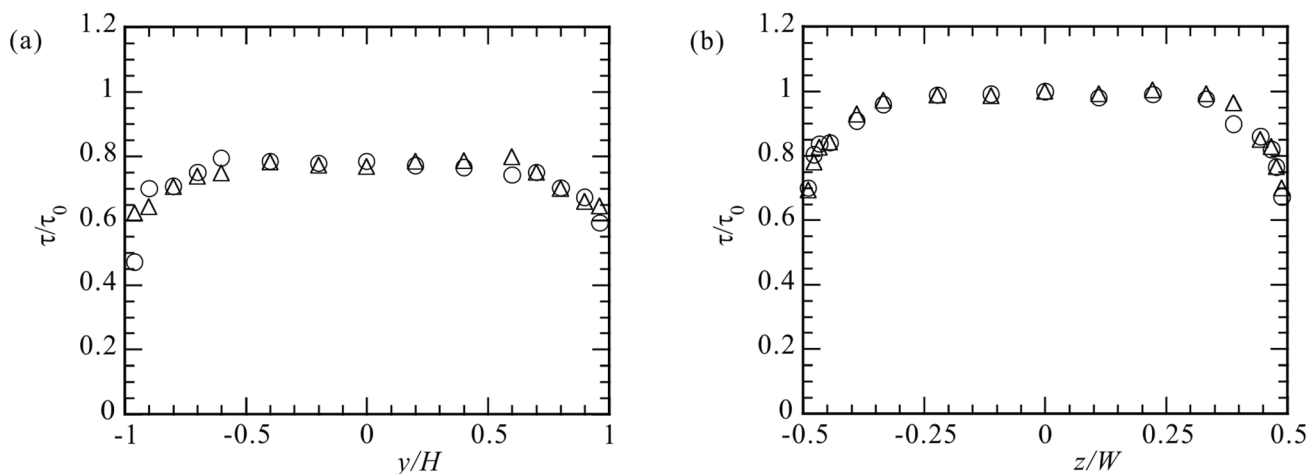
Fig. 8 Distributions of wall shear stress in the cross section of smooth channel, measured by a Preston tube. **a** y profiles at $z/W = -0.5$, **b** z profiles at $y/H = -1$. τ_0 represents wall shear stress at the channel

mid-span ($z = 0$). ○, $U_c = 5.8$ m/s ($U_b = 5.1$ m/s); △, $U_c = 8.4$ m/s ($U_b = 7.4$ m/s). The bulk velocity U_b was obtained from velocity measurements by hot-wire at $z = 0$

z-distributions of local friction measured by a Preston tube (diameter of 1.5 mm). We see that the local friction was about 80% of the value at the mid-span of the smooth channel τ_0 (Fig. 8a), while it was nearly uniform over 70% of the full span ($-0.35 \leq z/W \leq 0.35$) (Fig. 8b). These variations in the local friction provide the average shear stress over the channel cross section to be about 94% of the wall shear stress at the mid-span ($z = 0$) τ_0. Thus, in order to estimate the friction drag of the smooth surface properly, it is reasonable to make a correction to the friction estimated from the measured pressure drop, as

$$\tau_0 = 1.06\tau_{\text{smooth}} \tag{3}$$

in the present experiments. Figure 9 compares the friction factor C_f with the Dean's formula (Dean 1978). Here, Re_b represents the Reynolds number based on bulk velocity U_b obtained from the velocity profiles by hot-wire at $z = 0$. The comparison includes both experimental data with and without the correction. A good agreement was found between the present data with the correction by Eq. (3) and Dean's formula. Thus, we used τ_0 as the wall shear (friction) stress on the smooth surface to evaluate the drag reduction rate $\Delta\tau$. τ_0 was also used to calculate the friction velocity u_τ. In estimating $\tau_{\text{riblet}} - \tau_{\text{smooth}}$ in Eq. (2), on the other hand, it may be assumed that the friction stress is the same as that for the smooth-surface channel except the area on which riblet sheet was glued. Then, $\tau_{\text{riblet}} - \tau_{\text{smooth}}$ is given as,

$$\tau_{\text{riblet}} - \tau_{\text{smooth}} = -2H\left[\left(\frac{dp}{dx}\right)_{\text{riblet}} - \left(\frac{dp}{dx}\right)_{\text{smooth}}\right]. \tag{4}$$

In Fig. 10a, the drag reduction rate $\Delta\tau$ is depicted against the riblet-ridge spacing in wall units $s^+ = su_\tau/\nu$ for the
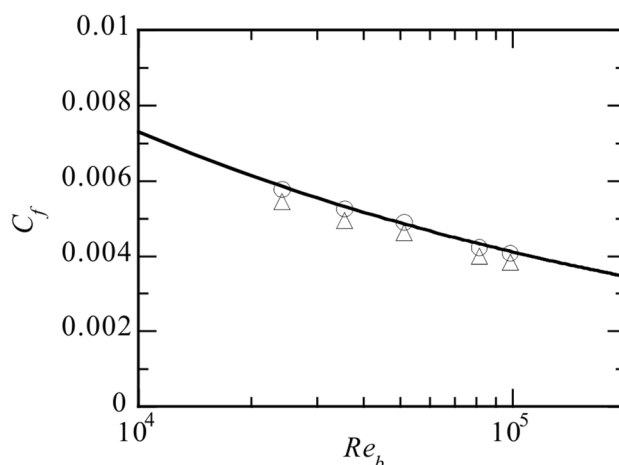

Fig. 9 Friction factor C_f versus bulk Reynolds number Re_b. △, C_f from Eq. (2); ○, C_f with Preston tube correction by Eq. (3). Solid line represents $C_f = 0.073\text{Re}_b^{-0.25}$ Dean (1978)

streamwise riblets ($\phi = 0°$). Here, for the riblet spacing s^+, the friction velocity (u_τ) measured on the smooth surface was used. The measurement was carried out more than 5 times for each s^+ and the regression curve was obtained for the measured data using a cubic polynomial. In Fig. 10b, the drag reduction rate averaged for each data set of s^+ with small variation $\Delta s^+ = \pm 1.5$ is displayed, where a bar for each data denotes the standard deviation of the measured drag reduction rate. The maximum drag reduction rate was about 7% for $s^+ = 18$ and the drag reducing effect of riblets ranged to $s^+ \approx 32$. This result is well correlated with that reported by Bechert et al. (1997) where the drag force was measured directly using a balance. It is also noted that the root of the groove cross section $(A_g^+)^{1/2}$ was 11.8 for $s^+ = 18$, which
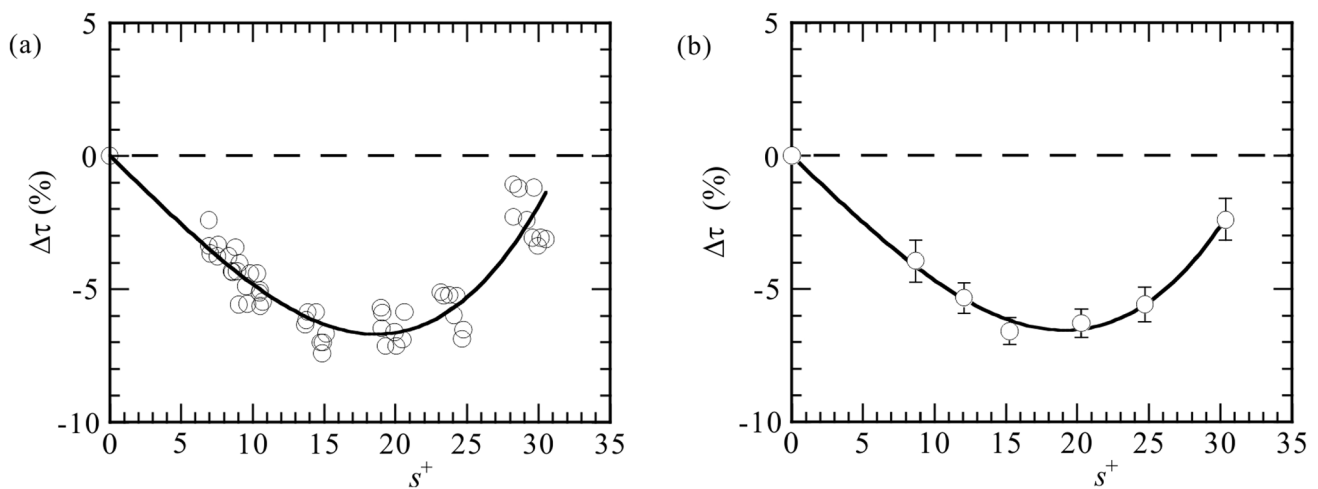
Fig. 10 Drag reduction rate $\Delta\tau$ for streamwise riblets. **a** All measured data. **b** Averaged values for $s^+ = 8.8 \pm 1.5$, 11.8 ± 1.5, 15.5 ± 1.5, 20.1 ± 1.5, 24.7 ± 1.5 and 30.4 ± 1.5. Error bars on each averaged value represents the variation range of data (the standard deviation). Solid lines represent regression curves for data

was close to the optical value 10.7 ± 1 proposed by Garcia-Mayoral and Jiménez (2011b).

3.3 Effects of yaw angle on drag reduction rate

We replaced the streamwise-riblet plate to the yawed-riblet plates ($\phi = 10°$, $12.5°$ and $15°$) and repeated measurements of the drag reduction rates in the similar way. In Fig. 11a, the drag reduction rate ($\Delta\tau$) is depicted against the riblet spacing (s^+) for $\phi = 10°$. The maximum drag reduction rate was about 7% at $s^+ \approx 18$ and the drag reduction effect of riblets was preserved up to $s^+ \approx 32$. These results were the same as those observed for the streamwise riblets. Thus, the drag reducing effect was still preserved without notable increase in pressure drag at least up to this yaw angle ($\phi = 10°$). For $\phi = 12.5°$, in Fig. 11b, on the other hand, the maximum drag reduction rate decreased to about 4% at around $s^+ = 15$ and turned to increase beyond $s^+ = 25$. For $\phi = 15°$, the drag reducing effect almost disappeared and the riblets worked as distributed roughness for $s^+ \geq 10$, as shown in Fig. 11c. The maximum drag reduction rate in each case is plotted against the yaw angle ϕ in Fig. 11d, showing that the drag reduction rate was attenuated steeply when ϕ exceeded $10°$. In this concern, we should refer to the early experiment by Walsh (1982) in which the yaw angle effect was examined for saw-tooth (triangle) riblets with ridge angle of $90°$. In his experiment, the drag reduction rate was not attenuated even at $\phi = 15°$ and the drag reduction occurred up to $\phi \approx 25°$. The difference in the yaw angle effect between the triangular and trapezoidal riblets can be attributed to the fact that the flow separation would be easier to occur at the riblet-ridges for the trapezoidal riblets with ridge angle of $30°$ when the ridge alignment is inclined to the main flow direction. To

confirm this, we examined the velocity profiles very close to the surface of yawed riblets carefully using a hot-wire anemometer.

Our attention was paid to a close comparison of the mean velocity profiles near the riblets between $\phi = 10°$ and $15°$ in Fig. 12a, b; Fig. 12b is a close-up of the profiles near the riblets ($y - y_{\text{tip}} \leq 4$ mm). The comparison was made with the same s^+ condition $s^+ = 15$ where the drag reduction rate was close to the maximum for $\phi = 0°$ and $10°$, while the drag had already turned to increase at $s^+ = 15$ for $\phi = 15°$. Here, the length of hot-wire sensor was 1 mm, while the spanwise scale of riblet grooves (or distance between the neighboring ridges) was 0.83 mm for the streamwise riblets and 0.86 mm for the yawed riblets of $\phi = 15°$. Considering that the effective length to sense the flow velocity was as large as 80% of the total sensor length (for hot-wire sensor with length-to-diameter ratio of 200) Champagne et al. (1967), the velocity profiles in Fig. 12a, b were considered to be those averaged over one groove. In the case of yawed riblets of $\phi = 10°$, it can be seen that the virtual origin where the mean velocity profile in the viscous sublayer tended to zero was located inside the grooves, as that observed in the case of streamwise riblets, indicating that a local mean cross-flow could exist inside grooves and also very close to riblet ridges. Note that according to the theoretical work by Luchini et al. (1991), the so-called protrusion height (Bechert and Bartenwerfer 1989) which is an offset between the virtual wall position and the riblet tip is about $0.2s$ (or $0.4h$) for streamwise riblets with the present groove geometry; the protrusion height of Luchini et al. was defined for a spanwise averaged velocity profile, whereas the virtual origin was near the tip of riblet-ridge for $\phi = 15°$. The latter fact indicates that flow separation occurred at riblet-ridges for the yawed riblets of

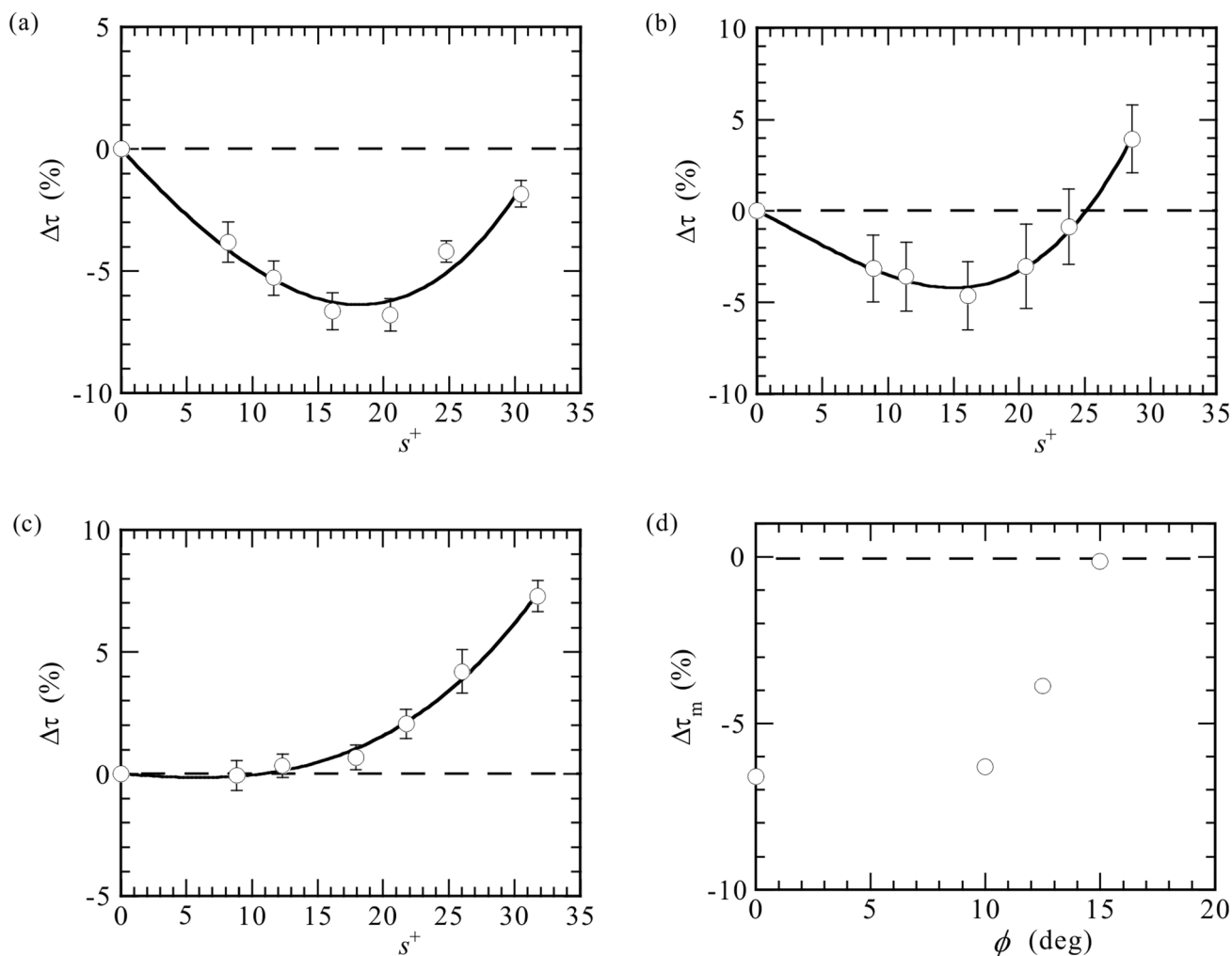**Fig. 11** Yaw angle effect of riblets on the drag reduction rate $\Delta\tau$. Drag reduction rate versus riblet spacing s^+ (in wall units) for **a** $\phi = 10°$, **b** $\phi = 12.5°$ and **c** $\phi = 15°$. **d** maximum drag reduction rate $\Delta\tau_{\mathrm{m}}$ versus ϕ. The measurements were conducted more than 5 times in all cases. Solid lines represent regression curves for measured data

$\phi = 15°$ and the separation-induced pressure drag canceled out the reduction in friction drag. In Fig. 12c, d, the y-distributions of the rms value u' near the riblets are compared between $\phi = 10°$ and 15°. The maximum rms values were almost the same for these two cases and smaller than that for the smooth surface case. Thus, the drag reduction rate was attenuated for $\phi = 15°$ despite the yawed riblets could suppress the turbulent intensity. It is also pointed out that the u'-distributions for $\phi = 15°$ was slightly shifted toward a higher y-position, corresponding to the change in the virtual origin observed in the velocity profile.

In order to further clarify impacts of misalignment of riblets on the near-wall turbulence structure, flows close to the streamwise and yawed riblets were examined using a rake probe with high spatial resolution; the sensor interval (= 0.6 mm) was slightly less than ridge spacing s (= 0.83 mm). Figure 13a, b illustrates the contours of

instantaneous streamwise velocity in the vicinity of the surface $y^+ \approx 7$ (where $U/U_{\mathrm{c}} \approx 0.3$) for the smooth and streamwise riblet cases at $Re_\tau = 1110$, where the riblet spacing was nearly optimal, i.e., $s^+ = 18.5$ (see Fig. 10). We see that development of low-speed streaks with spanwise spacing of about 5 mm (about 100 in wall unit) for the smooth surface case. For the case of riblets in Fig. 13b, on the other hand, small-scale velocity fluctuations were found markedly, especially along high-speed regions, although two-dimensional rollers due to a Kelvin–Helmholtz instability suggested from a direct numerical simulation by Garcia-Mayoral and Jiménez (2011a) were not identified. We performed two-dimensional spectral analyses for instantaneous streamwise velocity field thus obtained over the spanwise distance of 28.2 mm (about 600 in wall units) for streamwise riblets ($\phi = 0°$) and yawed riblets of $\phi = 10°$ and 15°.
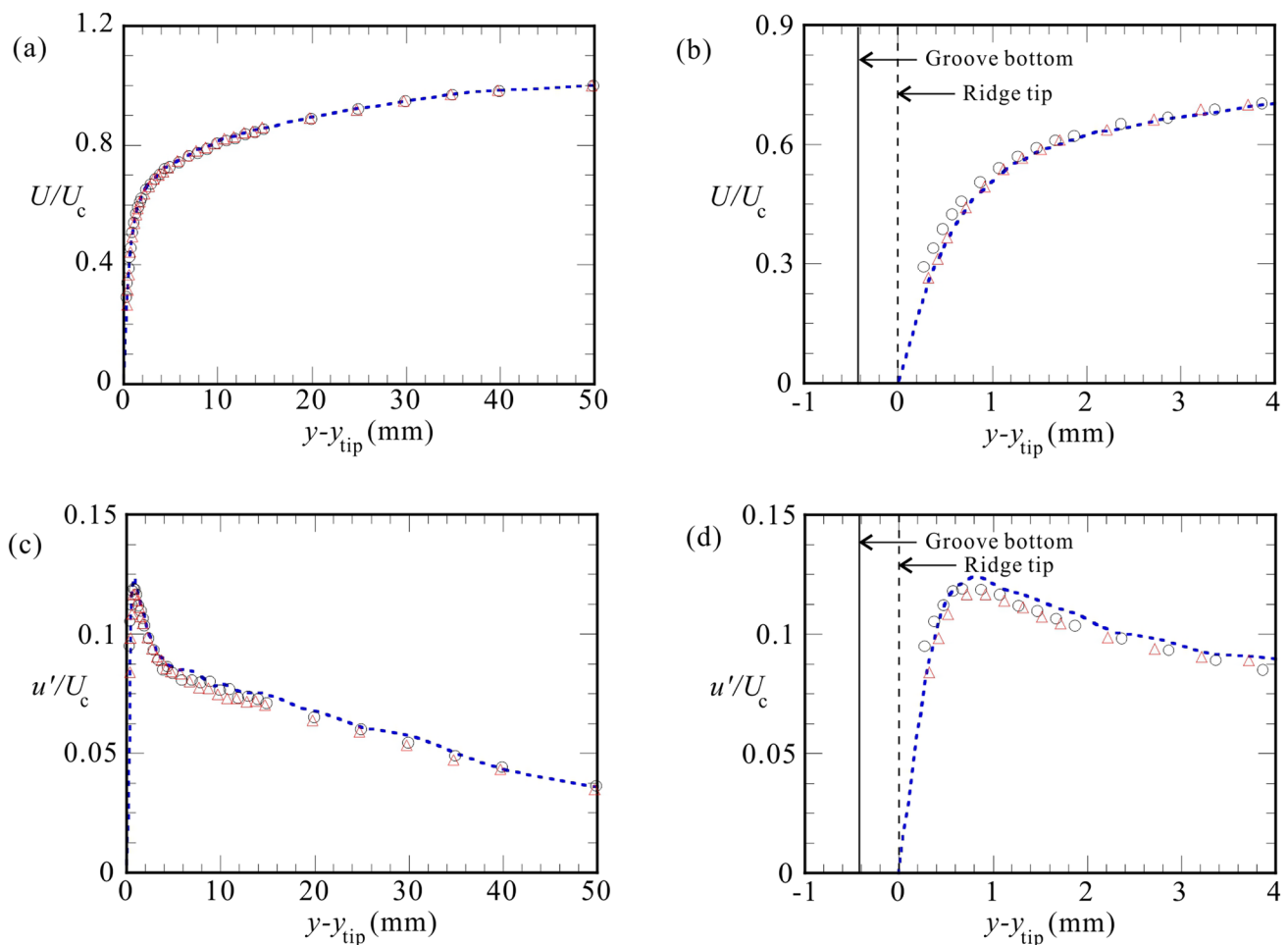
Fig. 12 Comparison of the y-distributions of **a, b** mean velocity U and **c, d** rms value u' near the riblets between $\phi = 10°$ (circle) and $15°$ (triangle) at $s^+ = 15.5$ ($Re_\tau = 930$). Dotted lines represent distributions in the smooth surface case at the same Reynolds number

In Fig. 14a–c, two-dimensional pre-multiplied power spectra of near-wall turbulence ($y^+ \approx 7$) for riblets with $\phi = 0°$, $10°$ and $15°$ are illustrated comparing to that for the smooth surface case at $Re_\tau = 1110$; where the riblet spacing $s^+ = 18.5$. Here, λ_x^+ and λ_z^+ denote streamwise and spanwise wavelengths in wall unit, respectively. Streamwise wavelength λ_x was obtained by means of Taylor's hypothesis assuming that all turbulent structures convected at $0.5U_c$. The maximum power at $(\lambda_x^+, \lambda_z^+) \approx (800, 100)$ in the pre-multiplied spectrum for the smooth surface corresponded to the typical streamwise and spanwise scales of low-speed streaks near the surface. Compared to the smooth surface case, the intensity of pre-multiplied power spectrum corresponding to low-speed streaks on the optimal-size riblets ($s^+ = 18.5$) became smaller, and the contours was shifted to the smaller wavelength side in $(\lambda_x^+, \lambda_z^+)$ although only slightly. These characteristics agreed with a numerical

simulation at the viscous breakdown stage (Garcia-Mayoral and Jiménez 2011a). Besides, comparing the pre-multi spectra for the $\phi = 10°$- and $15°$-yawed riblets to the streamwise-riblet cases, we could not find any notable difference between them. That is, the near-wall turbulence structure was little affected by the misalignment of riblets even for $\phi = 15°$. Thus, it is reasonable to infer that the drag reduction rate attenuated at $\phi = 15°$ was attributed to increase in pressure drag by the flow separation at the riblet-ridges.

4 Conclusion

Effects of the yaw angle on the drag reduction rate of riblets were examined experimentally using a turbulent wind channel for the trapezoidal riblets with ridge angle $30°$ and height-to-spacing ratio $h/s = 0.5$. The riblet-ridge spacing
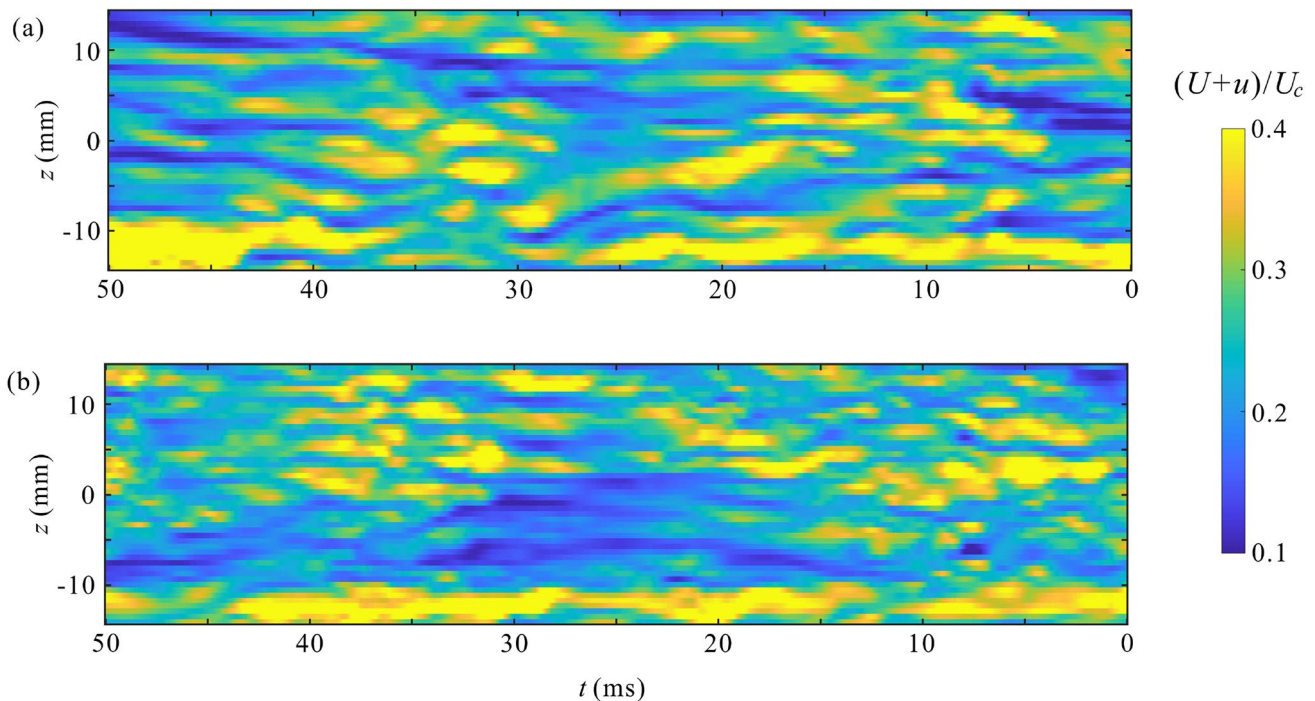
Fig. 13 Contour maps of instantaneous streamwise velocity $(U + u)$ measured by hot-wire rake at $y^+ \approx 7$ ($U/U_c \approx 0.3$) for $\mathrm{Re}_\tau = 1110$ ($s^+ = 18.5$ for riblets). **a** Smooth wall, **b** streamwise riblet. Note that time t is from right to left direction

in wall units s^+ was changed over 7–32 with controlling the channel center-line velocity and therefore the Reynolds number Re_τ ($= H u_\tau / \nu$) over 520–2100. Drag reduction rates were estimated by comparing the streamwise pressure gradients between turbulent channel flows with and without riblets. The ratio of the channel half depth to the riblet height H/h was 120. Such large H/h could reduce possible influences due to difference in the cross-sectional area between the smooth- and ribbed-surface channels. In addition, we used long riblet sheets with $40H$ in the streamwise direction to avoid possible effect of the surface transition from the smooth to ribbed surfaces on the measurements of drag reduction rate. These careful setups of the experiment enabled us to estimate the yaw angle effect of drag reduction rate with sufficient accuracy.

The maximum drag reduction rate was about 7% at around $s^+ \approx 18$ for the streamwise riblets. This drag reduction rate was maintained without any notable attenuation for $\phi \le 10°$. When ϕ exceeded $10°$, the drag reduction rate was attenuated steeply to about half at $\phi = 12.5°$ and the performance of riblets was almost lost at $\phi = 15°$. The effect of the yaw angle found for the trapezoidal riblets was rather different from the saw-tooth-riblet case reported by Walsh (1982): In the experiment for the saw-tooth riblets, the drag

reducing effect was not attenuated even at $\phi = 15°$ and was observed at least up to $\phi = 25°$. Thus, the yaw angle effect of riblets was highly dependent on the cross-sectional geometry of riblets.

The yaw angle effects on the drag reduction performance were further clarified by detailed comparisons of mean velocity profiles and turbulent structures near the ribbed surface between the yawed riblets of $\phi = 10°$ and $15°$ and the streamwise riblets. The turbulence intensity and pre-multiplied power spectra for the yawed riblets of $\phi = 10°$ and $15°$ exhibited no appreciable difference from those of the streamwise riblets, whereas the mean velocity profile showed an evidence of the flow separation very close to the ribbed surface for the yawed riblets of $\phi = 15°$. Thus, although the suppression effect of the turbulence structure near the ribbed surface was still maintained for misalignment of $\phi = 15°$, flow separation occurred at the riblet ridges, leading to the attenuation of drag-reduction rate due to increase in the pressure drag when ϕ increased to $15°$ for trapezoidal riblets with ridge angle of $30°$. These facts indicate that the critical yaw angle beyond which the drag-reducing effect is lost can also be found by investigating the shift of the virtual origin where the velocity profile in the viscous sublayer tends to zero.
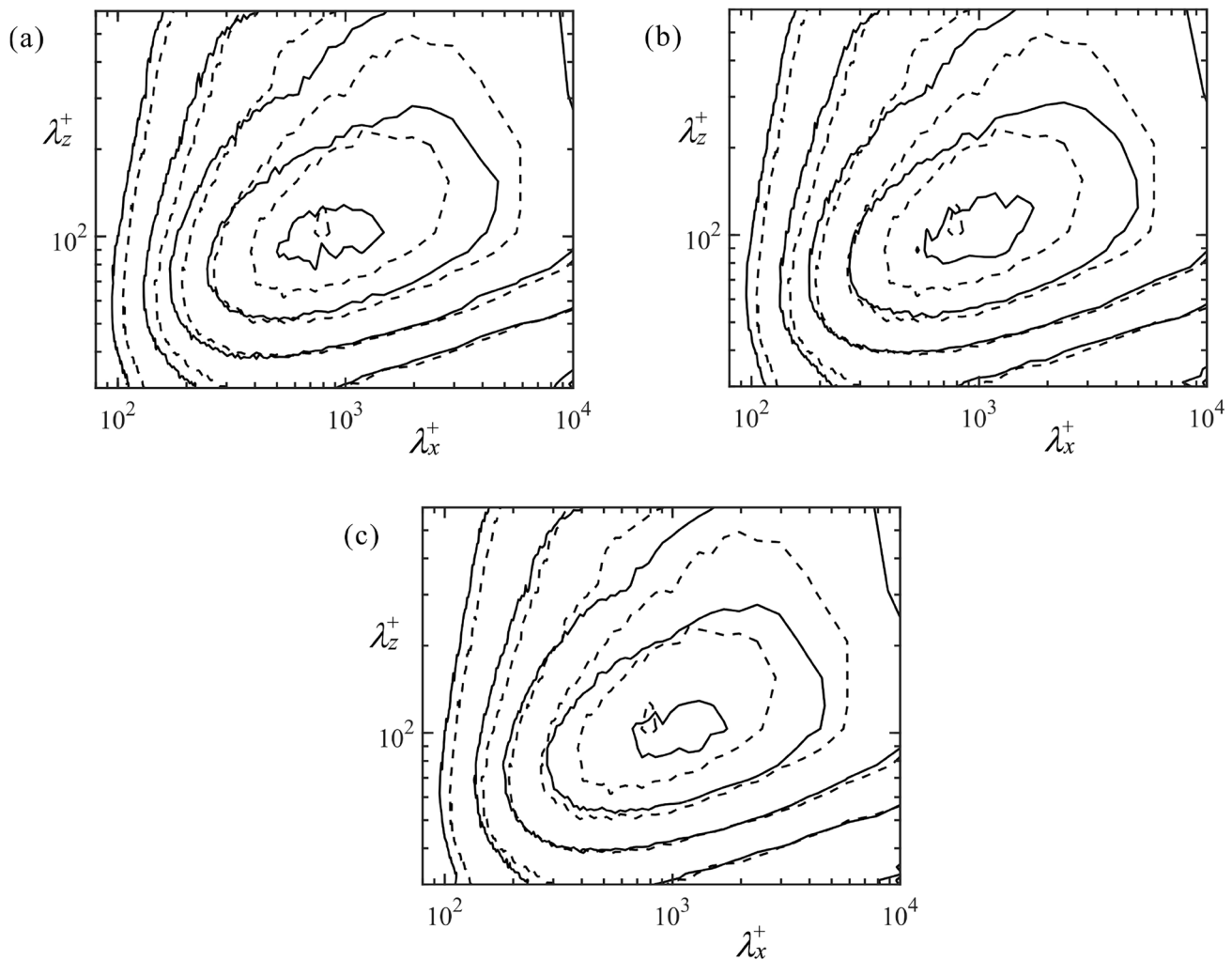
(a)

(b)

(c)

Fig. 14 Contour maps of the pre-multiplied two-dimensional power spectra of streamwise velocity fluctuations at $y^+ \approx 7$ ($U/U_c \approx 0.3$) for riblets of $s^+ = 18.5$ (solid lines) and smooth surface (dashed lines) at $\mathrm{Re}_\tau = 1110$. **a** $\phi = 0°$, **b** $10°$, **c** $15°$. Contour levels are 0.05, 0.2, 0.5, 1.2, 2.3, 3.8×10^{-5}

Availability of data and materials Data presented in this study will be available from the corresponding author upon reasonable request.

Declarations

Conflict of interest The authors declare that they have no conflict of interest.

Ethical approval Not applicable.

References

Bechert DW, Bartenwerfer M (1989) The viscous flow on surfaces with longitudinal ribs. J Fluid Mech 206:105–129. https://doi.org/10.1017/S0022112089002247

Bechert DW, Bruse M, Hage W, Van Der Hoeven JGT, Hoppe G (1997) Experiments on drag-reducing surfaces and their optimization with an adjustable geometry. J Fluid Mech 338:59–87. https://doi.org/10.1017/S0022112096004673

Cafiero G, Ius G (2022) Drag reduction in a turbulent boundary layer with sinusoidal riblets. Exp Thermal Fluid Sci 139:110723. https://doi.org/10.1016/j.expthermflusci.2022.110723

Champagne FH, Sleicher CA, Wehrmann OH (1967) Turbulence measurements with inclined hot-wires part 1. Heat transfer experiments with inclined hot-wire. J Fluid Mech 28(1):153–175. https://doi.org/10.1017/S002211206700196X

Choi K-S (1989) Near-wall structure of a turbulent boundary layer with riblets. J Fluid Mech 208:417–458. https://doi.org/10.1017/S0022112089002892

Choi H, Moin P, Kim J (1993) Direct numerical simulation of turbulent flow over riblets. J Fluid Mech 255:503–539. https://doi.org/10.1017/S0022112093002575

Dean RB (1978) Reynolds number dependence of skin friction and other bulk flow variables in two-dimensional rectangular duct flow. J Fluids Eng 100(2):215–223. https://doi.org/10.1115/1.3448633

Deyn LH, Gatti D, Frohnapfel B (2022) From drag-reducing riblets to drag-increasing ridges. J Fluid Mech 951:16. https://doi.org/10.1017/jfm.2022.796

Sundaram S, Viswanath PR, Subaschandar N (1999) Viscous drag reduction using riblets on a swept wing. AIAA J 37(7):851–856. https://doi.org/10.2514/2.7533

Garcia-Mayoral R, Jiménez J (2011a) Hydrodynamic stability and breakdown of the viscous regime over riblets. J Fluid Mech 678:317–347. https://doi.org/10.1017/jfm.2011.114

Garcia-Mayoral R, Jiménez J (2011b) Drag reduction by riblets. Philos Trans R Soc A 678:1412–1427. https://doi.org/10.1098/rsta.2010.0359

Hage W, Bechert DW, Bruse M (2001) Yaw angle effects on optimaized riblets. Notes Numer Fluid Mech 76:278–285. https://doi.org/10.1007/978-3-540-45359-8_29

Inasawa A, Takagi S, Asai M (2020) Improvement of the signal-to-noise ratio of the constant-temperature hot-wire anemometer using the transfer function. Meas Sci Technol 31(5):055302. https://doi.org/10.1088/1361-6501/ab6916

Inasawa A, Takagi S, Asai M (2021) Experimental investigation of the effects of length-to-diameter ratio of hot-wire sensor on the dynamic response to velocity fluctuations. Exp Fluids 62:92. https://doi.org/10.1007/s00348-020-03131-1

Luchini P, Manzo F, Pozzi A (1991) Resistance of a grooved surface to parallel flow and cross-flow. J Fluid Mech 228:87–109. https://doi.org/10.1017/S0022112091002641

Moser RD, Kim J, Mansour NN (1999) Direct numerical simulation of turbulent channel flow up to $Re_\tau = 590$. Phys Fluids 21:943–945. https://doi.org/10.1063/1.869966

Okabahashi K, Yamada Y, Asai M (2015) Parametric analysis of flow over sinusoidal riblets. Proc Turbul Shear Flow Phenom 9:237

Okabayashi K (2017) Direct numerical simulation for investigation on yaw angle effects on riblets. Trans Jpn Soc Mech Eng 12(1):0008. https://doi.org/10.1299/jfst.2017jfst0008

Patel VC (1965) Calibration of the Preston tube and limitations on its use in pressure gradients. J Fluid Mech 23(1):185–208. https://doi.org/10.1017/S0022112065001301

Peet Y, Sagaut P (2009) Theoretical prediction of turbulent skin friction on geometrically complex surface. Phys Fluids 21:105105. https://doi.org/10.1063/1.3241993

Preston JH (1954) The determination of turbulent skin friction by means of pitot tubes. Aeronaut J 58(518):109–121. https://doi.org/10.1017/S0368393100097704

Sasamori M, Mamori H, Iwamoto K, Murata A (2014) Experimental study on drag-reduction effect due to sinusoidal riblets in turbulent channel flow. Exp Fluids 55:1828. https://doi.org/10.1007/s00348-014-1828-z

Sasamori M, Iihama O, Mamori H, Iwamoto K (2017) Parametric study on a sinusoidal riblet for drag reduction by direct numerical simulation. Exp Fluids 99:47–69. https://doi.org/10.1007/s10494-017-9805-2

Suzuki Y, Kasagi N (1994) Turbulent drag reduction mechanism above a riblet surface. AIAA J 32(9):1781–1790. https://doi.org/10.2514/3.12174

Van Buren T, Floryan D, Ding L, Hellström LHO, Smits AJ (2020) Turbulent pipe flow response to a step change in surface roughness. J Fluid Mech 904:38. https://doi.org/10.1017/jfm.2020.704

Walsh MJ (1980) In: Hough GR (ed) Drag characteristics of V-groove and transverse curvature riblets. Viscous flow drag reduction. AIAA, New York, pp 168–184. https://doi.org/10.2514/5.9781600865466.0168.0184

Walsh MJ (1990) In: Bushnell DM, Hefner JN (ed) Riblets. Viscous drag reduction in boundary layers. AIAA, New York, pp 203–261. https://doi.org/10.2514/5.9781600865978.0203.0261

Walsh MJ (1982) Turbulent boundary layer drag reduction using riblets. AIAA Paper 82–0169. https://doi.org/10.2514/6.1982-169

Walsh MJ, Lindemann AM (1984) Optimization and application of riblets for turbulent drag reduction. AIAA Paper 84–0347. https://doi.org/10.2514/6.1984-347

Walsh MJ, Weinstein LM (1978) Drag and heat transfer of surface with small longitudinal fins. AIAA Paper 78–1161. https://doi.org/10.2514/6.1978-1161

Walsh MJ (1983) Riblets as a viscous drag reduction technique. AIAA J 21(4):485–486. https://doi.org/10.2514/3.60126

Wang J, Lan S, Chen G (2000) Experimental study on the turbulent boundary layer flow over riblets surface. Fluid Dyn Res 27(4):217–229. https://doi.org/10.1016/S0169-5983(00)00009-5